




# Damage assessment in single-nave churches and analysis of the most recurring mechanisms after the 2016–2017 central Italy earthquakes

F. Ceroni<sup>1</sup> · C. Casapulla<sup>2</sup>  · E. Cescatti<sup>3</sup> · V. Follador<sup>3,4</sup> · A. Prota<sup>2</sup> · F. da Porto<sup>3</sup>

Received: 20 April 2022 / Accepted: 22 August 2022 / Published online: 5 September 2022  
© The Author(s) 2022

## Abstract

Assessment of churches based on empirical data at a territorial scale is a suitable tool to have an overview of the seismic behaviour of this peculiar structural typology and to evaluate their current state of vulnerability. Fragility and vulnerability curves are also aimed to perform the analysis of different seismic scenarios. The paper presents a detailed typological analysis of 633 single-nave churches, as a selected subset of the database previously examined by the authors, with the aim of evaluating more in detail the influence of some parameters, such as masonry typology, church dimensions and presence of the bell tower, on the vulnerability of the overall church. Then, specific analyses are carried out to assess the influence played by single mechanisms on the definition of the overall damage index, with the focus of providing qualitative evaluations and explicit vulnerability and fragility curves related to the most recurring and significant collapse mechanisms. This is an original contribution of the paper in the field of the vulnerability assessment of churches, since nowadays little information is available in the literature about the damage levels related to specific mechanisms, while most attention is still focused on global damage.

**Keywords** Churches · Masonry · Post-earthquake survey · Damage · Collapse mechanisms · Fragility curves · Vulnerability curves

---

✉ C. Casapulla  
claudia.casapulla@unina.it

<sup>1</sup> Department of Engineering, University of Napoli ‘Parthenope’, Naples, Italy

<sup>2</sup> Department of Structures for Engineering and Architecture, University of Napoli Federico II, Naples, Italy

<sup>3</sup> Department of Geosciences, University of Padova, Padua, Italy

<sup>4</sup> Department of Civil, Environmental, Architectural Engineering and Mathematics, University of Brescia, Brescia, Italy

## 1 Introduction

Vulnerability of masonry churches is higher than that of ordinary buildings, as proven by many post-earthquake reconnaissance and numerical analyses on this specific building typology (Doglioni et al. 1994; Lagomarsino and Podestà 2004a; da Porto et al. 2009; Lagomarsino 2012; Sorrentino et al. 2014; Taffarel et al. 2016; Canuti et al. 2021, Penna et al. 2019; Cescatti et al. 2020; Salzano et al. 2022). This is mainly due to the peculiar architectural layout and geometry of this type of buildings and, in some cases, to the poor mechanical properties of masonry. In particular, the structural layout of a church is characterized by several drawbacks, such as: i) the presence of few, perimeter load-bearing walls (façade, side walls, etc.); ii) the absence of an internal bracing systems or shear walls; iii) the presence of thrusting elements (e.g. arches, vaults); iv) the presence of a single horizontal diaphragm at the top and, often, a pitched roof, usually not designed to redistribute seismic actions. In many cases, it also occurs that the load-bearing walls are very slender.

Because of their structural configuration, churches often have limited capacity to distribute and counteract horizontal actions and are prone to develop instability phenomena or activate out-of-plane mechanisms, also related to the wall slenderness. In addition, the architectural layouts of some typical parts of churches, as side chapels, domes, apses, etc., make them also vulnerable to horizontal actions because of torsional or shear effects. Therefore, the seismic response of churches can be described following recurring models, which are related to damage and collapse mechanisms of single portions of the building. These parts are the so-called macro-elements, and consist of separate structural portions that show an almost autonomous structural behaviour, with specific damage mechanisms (Doglioni et al. 1994), as typically occurs in ordinary masonry buildings, too (D'Ayala and Speranza 2003; Casapulla et al. 2021). Façade, bell tower, apse, side chapels, etc., are typical examples of macro-elements in churches.

Currently, 28 damage mechanisms, connected to 9 macro-elements, are recognised and collected in the A-DC form, used in Italy for the damage survey of churches after seismic events (PCM-DPC-MiBAC 2006). Once the form is filled out during the post-earthquake phase, a global damage index can be calculated as the mean damage related to each possible mechanism of the examined church, normalized to 1. As observed in the past, these mechanisms may have higher or lower probability to be activated, depending on the specific vulnerability of the related macro-elements and, thus, the damage related to each mechanism can be useful to highlight the most influential macro-elements on the overall vulnerability of the church. For instance, during past earthquakes it has been observed that damage is often concentrated in the top section of the façade, in the vaults and in the gable of bell towers (da Porto et al. 2009; Sorrentino et al. 2014; Cescatti 2016). Therefore, it could be argued that the damage related to these mechanisms should represent an important rate of the overall damage.

Generally, the results of post-earthquake surveys are statistically examined to derive empirical vulnerability and fragility curves, which can be used to predict the overall damage state of churches as a function of the registered macro-seismic intensity (Lagomarsino and Podestà 2004b; De Matteis et al. 2019; Zizi et al. 2021) or of the peak ground acceleration (Canuti et al. 2021, De Matteis and Zizi 2019; Penna et al. 2019; Cescatti et al. 2020; 2021; Morici et al. 2020). As an alternative approach, Marotta et al. (2018) have introduced new synthetic indices able to summarise the damage related to several mechanisms, or the global damage to the church, on the basis of some vulnerability indicators (i.e. structural details and presence of resistant elements), also adopted in a new survey form proposed

by Lagomarsino et al. (2019). Similarly, Marotta et al. (2021) have derived parametric fragility curves for churches, based on the damage observed on 21 mechanisms, taking into account vulnerability factors that worsen or improve the seismic response. On the other hand, fragility functions for single local mechanisms have been derived for both church façades (Giresini et al. 2018; Solarino and Giresini 2021) and unreinforced masonry buildings (Nale et al. 2021), using nonlinear dynamic analyses and probabilistic approaches. Notwithstanding, the literature on this topic is still rather limited, and the specific relevance of each mechanism on the damage to the whole church is still an open issue.

Therefore, with reference to a homogenous class of churches, i.e. a stock of churches of a certain typology, one of the aims of this work is to separately analyse the different mechanisms involving the macro-elements, to establish not only the global vulnerability of the selected churches, but also the vulnerability of the single macro-elements affected by all the activable mechanisms.

The homogeneous class herein considered is a group of 633 single-nave churches hit by the 2016–17 Central Italy seismic sequence, representing a subset of the larger database of 990 churches previously analysed by the same research group (Cescatti et al. 2020). This church typology has the following features: rectangular plan with single nave, masonry made of stones or bricks, absence of lateral chapels and/or transepts, possible presence of apse, gabled façade, presence of a bell gable or a bell tower.

The observational data are herein analysed to develop damage probability matrices and fragility curves related to slight, moderate, and severe damage states (DS), with reference to both the global behaviour of the church and the most recurring failure mechanisms. The latter aspect provides a meaningful contribution to the study and characterization of the vulnerability and damage related to single mechanisms and highlights which mechanisms need to be more carefully examined during post-seismic surveys.

## 2 Main characteristics of single-nave churches

### 2.1 Shape and building materials

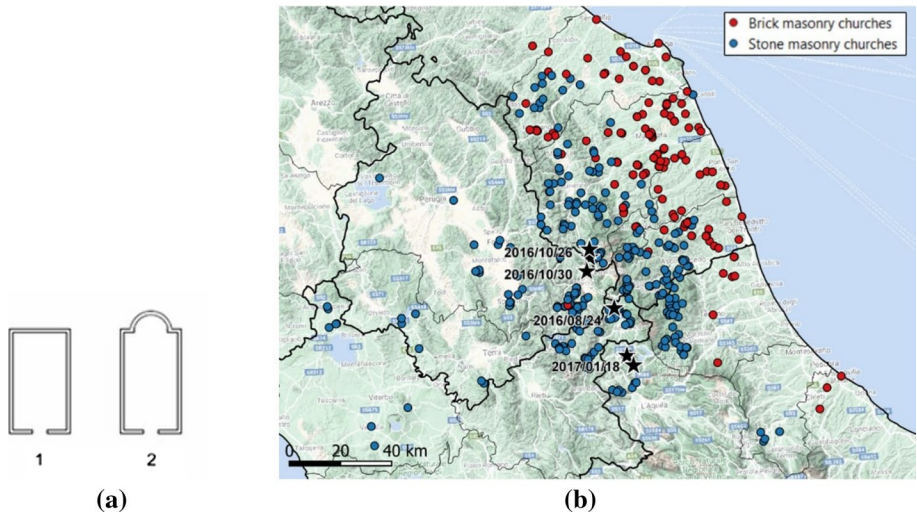
The database of churches examined in this study includes 633 single-nave masonry churches, which are characterized by the typical rectangular plan shapes reported in

Figure 1a, with (type 2) or without (type 1) apse.

Figure 1b shows the geographical distribution of the single-nave churches made of stone masonry (blue plots) and clay brick masonry (red plots), and evidences a territorial influence on the choice of the building material. Clay brick masonry churches are, indeed, distributed along the coast, whereas stone masonry churches are mainly found on hill and mountain areas. Such a simplified classification of masonry typologies (stone and clay bricks) is based on some information available from the survey forms, and two examples of such types are reported in Fig. 2.

The masonry type is identified for 549 churches: 146 are made of clay brick masonry and 403 of stone masonry. Conversely, data on the masonry type are not available for the remaining 84 churches, as they could not be inferred from the available documentation (A-DC form, survey notes and photos).

Within these 549 single-nave churches, Fig. 3a shows that the most common façade has a gabled shape (Fig. 3b), with an occurrence of about 70% for both clay brick and stone



**Fig. 1** **a** Plan shapes of the inspected single-nave churches; **b** geographical distribution of the single-nave churches according to the masonry typologies

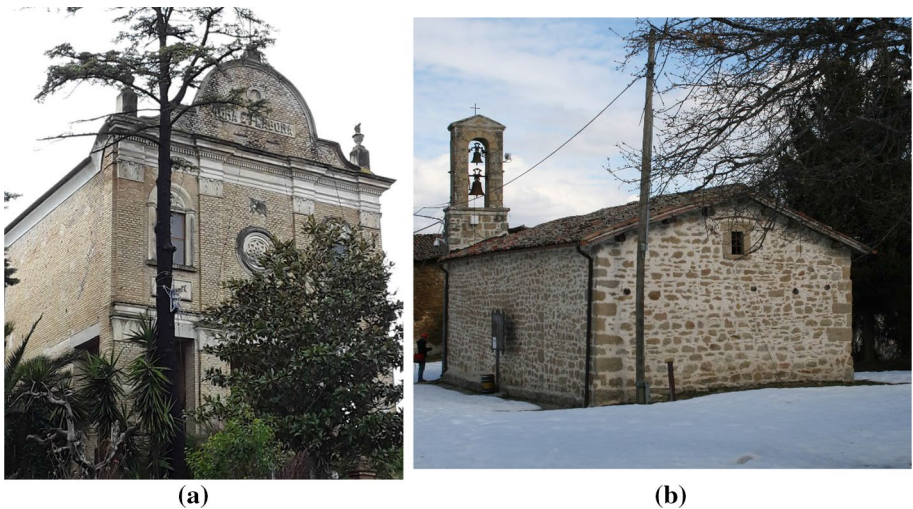


**Fig. 2** **a** Example of a clay brick masonry church: San Callisto Church (Manoppello, Pescara, Abruzzo); **b** example of a stone masonry church: San Lorenzo Church (Accumoli, Rieti, Lazio).

masonry churches. For about 7% of this sample, information about the façade shape is not available, again because this data is not reported in the survey documentation.

## 2.2 Tower bell typology

Among the 633 single-nave churches of the investigated stock, three main typologies of bell towers are identified: the ‘bell gable’ (Fig. 4a), the ‘integrated’ bell tower, which can

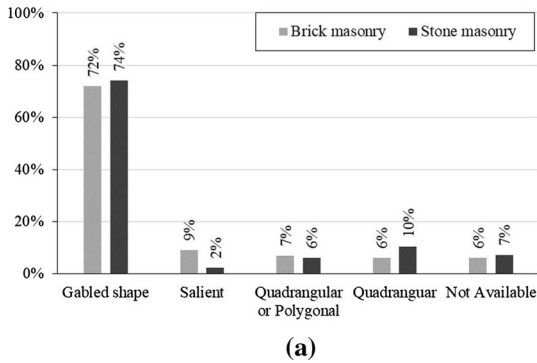


**Fig. 3** **a** Statistical distribution of the façade type for 146 brick masonry churches and 403 stone masonry churches; **b** example of a gabled façade

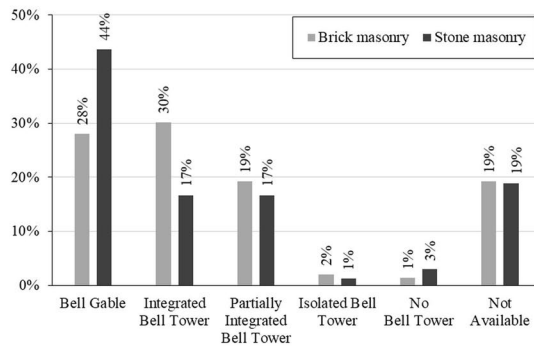


**Fig. 4** **a** Stone masonry bell gable in the Santa Maria Assunta Church (Funtoli, Ascoli Piceno); **b** integrated brick masonry bell tower in the San Paterniano Church (San Severino Marche, Macerata); **c** partially integrated brick masonry bell tower in the San Nicola Church (Casacanditella, Chieti); **d** isolated bell tower in the San Giovanni Church (Cascia, Perugia); **e** statistical distribution of bell tower typologies for 146 brick masonry churches and 403 stone masonry churches

be joined to different parts of the church (Fig. 4b-c), and the ‘isolated’ bell tower (Fig. 4d). It is worth noting that information about the bell tower typology is not available for a relevant number of churches of the whole database (20%, 129 churches).

Figure 4e shows that most of the churches have a ‘bell gable’ (28% of the brick and 44% of the stone masonry churches) followed by ‘integrated’ bell towers (30% of the brick and 17% of the stone masonry churches) and ‘partially integrated’ bell towers (19% of the brick and 17% of the stone masonry churches). Only in few cases (1–2%, i.e. 8 cases), the bell towers are completely separated from the church.

A study of the correlation between the overall dimensions of each church (church maximum height and its covered surface area) and the types of bell tower/gable has also been carried out. In particular, the combined information about bell tower typology and church volume is available for 206 cases of bell gables, 194 cases of integrated bell towers, and 8 cases of isolated bell towers. Figure 5a plots the volume distribution of 204 out of 206 churches with bell gable, and Fig. 5b plots the volume distribution of 174 out of 194 churches with integrated bell tower. Since only 8 churches have an isolated bell tower, the number is too limited to be considered statistically significant. The churches with integrated bell tower have a volume distributed in the range 0–5000 m<sup>3</sup>, whereas the churches with bell gable are characterized by smaller volumes, i.e. lower than 1200 m<sup>3</sup> for most of them (83%).

Frequency data function of the volume is fitted by a lognormal distribution, obtaining a median value of 288 m<sup>3</sup> for the churches with bell gable and of 1920 m<sup>3</sup> for those with integrated bell tower. Moreover, for the churches with bell gable, the 84<sup>th</sup> percentile is 1205 m<sup>3</sup>, whereas for integrated bell tower, it is 3856 m<sup>3</sup>. As expected, these results highlight that churches with larger dimensions are usually characterized by the presence of an integrated or isolated bell tower, whereas smaller churches only present a bell gable.

### 3 Damage recorded after the 2016–17 seismic sequence

An accurate study of the damage index as a function of the macro-seismic intensity evaluated according to MCS,  $I_{MCS}$ , and of the peak ground acceleration, PGA, is presented in the following. The PGA values are evaluated by the shake-maps interpolations, whereas the  $I_{MCS}$  are derived from the INGV (National Institute of Geophysics and Volcanology) reports. For each church, both  $I_{MCS}$  and PGA values were selected according to the strongest event suffered during the seismic sequence, up to the date of the inspection.

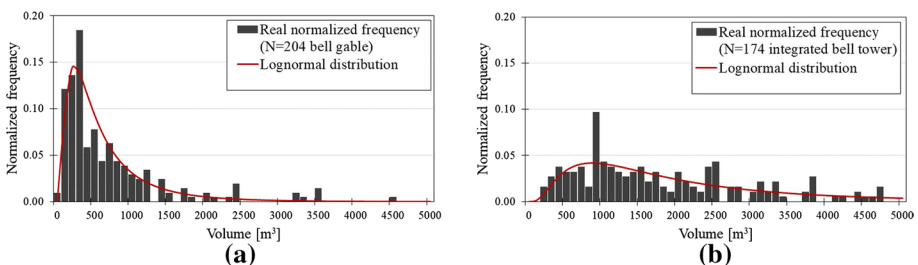


**Fig. 5** Volume distribution for: **a** churches with bell gable and **b** churches with integrated and isolated bell towers

The global mean damage index is defined according to the following well-known formulation:

$$i_d = \frac{1}{5} \frac{\sum_{k=1}^n d_k}{n} \tag{1}$$

where  $n$  is the number of activated mechanisms, all assumed with the same weight, and  $d_k$ , variable between 0 and 5, is the level of damage recorded for each of the 28 damage mechanisms reported in the A-DC form (PCM-DPC-MiBAC 2006, reapproved by MiBACT 2015), which are usually drawn up during in-situ surveys in the post-seismic emergency.

Figure 6a shows the values of  $i_d$  recorded for all the single-nave masonry churches, while Fig. 6b and Fig. 6c consider the different trends for clay brick and stone masonry churches, respectively. It can be noted that most of the brick masonry churches are characterized by low values of PGA (lower than 0.2 g) and macro-seismic intensity, because of the geographical distribution of the brick masonry churches, mainly along the coast (Fig. 1b). Consequently, they are characterized by low damage indexes (lower than 0.5), also in comparison with the stone masonry churches. If we consider the same acceleration range (i.e. 0–0.15 g) for the two classes of churches (stone and brick masonry), the level of the observed damage seems

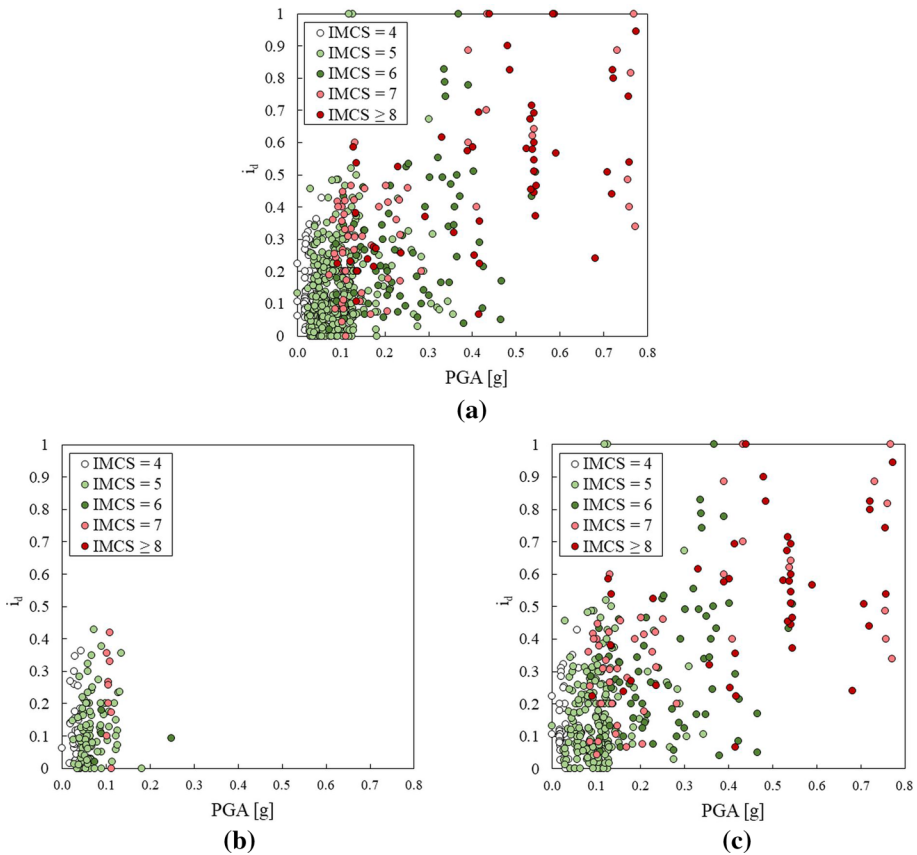


**Fig. 6** Damage index distribution vs. PGA and for different MCS macro-seismic intensities for **(a)** 633 single-nave masonry churches; **b** 146 brick masonry churches; **c** 403 stone masonry churches

apparently similar and, therefore, more accurate analyses are necessary to define an eventual trend, or a different response, of the churches made of the two masonry types.

Additionally, Fig. 7 shows the different dimensions of the stone and the brick masonry churches of the analysed stock. Most of the stone masonry churches (Fig. 7a) are, indeed, characterized by small dimensions (66% have an average area lower than 130 m<sup>2</sup>), while brick masonry churches (Fig. 7b) have a more homogenous distribution of the plan area in the range 0–600 m<sup>2</sup>. Such condition, in addition to the location far from the main centres, might indicate that most of the churches of this class have a limited ecclesiastical importance, are scarcely frequented and, for these reasons, may have been poorly maintained before the occurrence of the seismic sequence.

## 4 Assessment of global mean damage for the single-nave churches class

### 4.1 Global mean damage as a function of macro-seismic intensity

A well-known methodology for estimating the mean damage correlated with the seismic input is provided by Lagomarsino and Podestà (2004b), derived from the analysis of damages observed on the Umbria and Marche churches after the 1997 Umbria-Marche seismic sequence. Such a method is based on the assessment of a vulnerability index for each church, which is obtained as the sum of the typological vulnerability indexes, related to the II level form (DPCM 2011, GNDT-DISEG 2004) and a vulnerability score, assigned to some relevant parameters of the construction. Nevertheless, since the vulnerability index was not evaluated during the in-situ inspections of the Central Italy churches, the global mean damage index is herein calculated according to Cescatti et al. (2021) as follows:

$$i_D = 0.5 \cdot [1 + \tanh(\alpha \cdot I_{MCS} - \beta)] \quad (2)$$

where  $I_{MCS}$  is the MCS macro-seismic intensity (Sieberg 1930), and  $\alpha$  and  $\beta$  are the correlation parameters that implicitly consider the intrinsic vulnerability of the structures of a given class and can be obtained through a best fitting procedure with observational data (Cescatti et al. 2021).

Formulations like Eq. (2) are widely used and validated in the literature to predict average damage and, thus, to represent the vulnerability of masonry churches. Other approaches, such as those based on binomial and lognormal distributions, have been

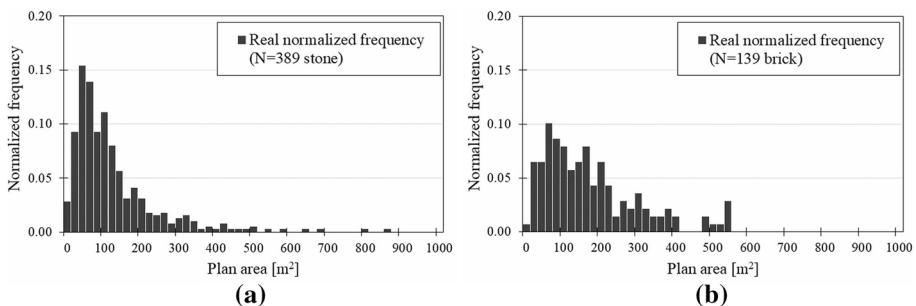


**Fig. 7** Statistical distribution of plan area of the **a** stone masonry churches and **b** brick masonry ones



evaluated at a preliminary stage of this work, as well as the possibility of carrying out a linear regression, but with less reliable results than those obtained with the method followed herein. In other works, Marotta et al. (2018,2021) have adopted a linear regression on other domains, Morici et al. (2020) have used a maximum likelihood estimation, whereas Lagomarsino et al. (2019) have proposed a Beta cumulative distribution.

Based on the data derived by the survey forms, mean damage can be derived as a function of  $I_{MCS}$  and the vulnerability curve is given by the best fitting of Eq. (2) on the experimental data. First, the 633 single-nave churches are subdivided in subgroups according to the assigned macro-seismic intensities, as reported in Table 1, where the number of churches,  $n_c$ , falling in each subgroup is indicated.

Then, for each value of  $I_{MCS}$ , the mean damage index observed for the  $n_c$  churches subjected to  $I_{MCS}$  is computed according to the following equation:

$$i_{d,mean}(I_{MCS}) = \frac{\sum_{i=1}^{n_c} i_d(I_{MCS})}{n_c} \tag{3}$$

Table 1 lists the mean damage index as a function of  $I_{MCS}$  for the whole database of single-nave churches and for the two subsets of brick and stone masonry churches.

In Fig. 8, the observed mean damage for the single-nave churches is reported versus  $I_{MCS}$  for the whole database (633 churches Fig. 8a) and separately for the stone (403 data) and clay brick (146 data) masonry churches (Fig. 8b).

Figure 8 shows that non-negligible observed damage is present also for low intensities. This could be partially caused by the presence of pre-existing damage, not correctly recognized by surveyors. It could also occur that damaged churches are over-represented, compared to the entire set of churches in the area affected by the earthquakes, although inspections on special classes of buildings, such as churches, are generally carried out in a thorough manner, including all buildings. Conversely, it is worth noting that the evaluation of the macro-seismic intensity is based on the average damage observed in all the buildings of the area, and not on the specific damage suffered by the churches, that are characterized, as above-mentioned, by higher vulnerability (Salzano et al. 2022).

**Table 1** Splitting of the database according to different MCS macro-seismic intensities

IMCS	All single-nave churches		Brick masonry churches		Stone masonry churches	
	$n_c$	$i_{d,mean}$	$n_c$	$i_{d,mean}$	$n_c$	$i_{d,mean}$
IV	106	0.117	42	0.114	47	0.139
V	256	0.128	76	0.113	142	0.141
V-VI	87	0.213	15	0.151	60	0.243
VI	36	0.208	3	0.102	30	0.229
VI-VII	36	0.385	1	0.093	34	0.398
VII	35	0.364	7	0.225	24	0.435
VII-VIII	27	0.358	2	0.262	24	0.362
VIII	21	0.379	–	–	15	0.438
VIII-IX	7	0.616	–	–	7	0.616
IX	10	0.542	–	–	10	0.542
IX-X	5	0.761	–	–	3	0.602
X	7	0.564	–	–	7	0.564

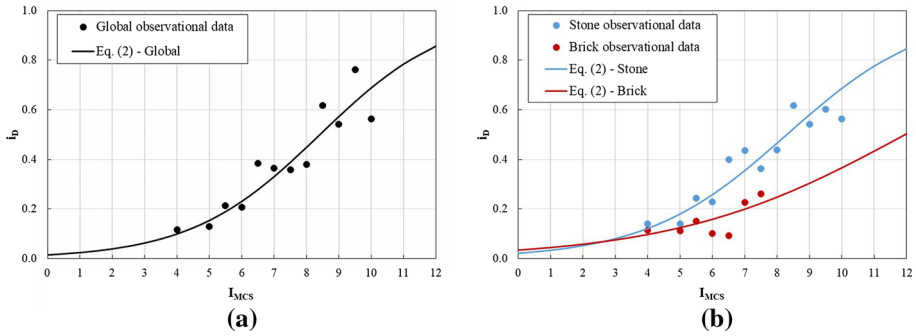


**Fig. 8** Observed and predicted mean damage indexes in single-nave churches vs.  $I_{MCS}$  for the: **a** whole data-base (633 churches); **b** stone (403) and brick (146) masonry churches

The  $\alpha$  and  $\beta$  correlation parameters of Eq. (2) are obtained through a least-squares fitting procedure with reference to the three datasets of  $i_{d,mean}$  plotted in Fig. 8. The values of  $\alpha$  and  $\beta$  are summarized in Table 2 and the curves of the predicted mean damage index  $i_D$  given by Eq. (2), using the fitted values of  $\alpha$  and  $\beta$ , are superimposed to the observed data in Fig. 8. Table 2 also reports the RSS parameter, i.e. the residual sum of squares of the observed  $i_{d,mean}$  values versus the  $i_D$  values predicted by Eq. (2), weighted on the number of fitted points per each macro-seismic intensity range.

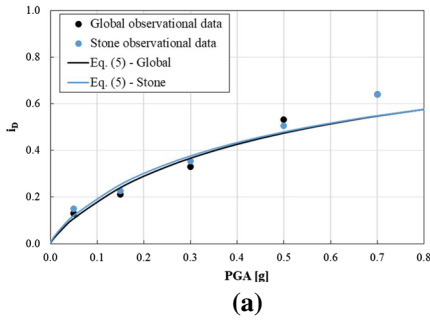
Figure 8b shows that the mean damage to brick masonry churches is lower than that of the stone ones, more clearly than the graphs presented in Sect. 3. Nevertheless, it is worth noting that the smaller number of observational data available for the brick masonry churches and their localization mainly close to the coast, i.e. quite far away from the epicentres, might make the observed damage not reliable for such a typology, especially for the highest  $I_{MCS}$ , and further data, as well as further typological characterization, are needed to confirm or not this observation.

### 4.2 Global mean damage as a function of PGA

The observed mean damage index is also plotted in Fig. 9 vs. the PGA values, again for the whole sample (633 data, black dots) and for the 403 stone masonry churches only (403 data, cyan dots). Also in this case, the damage observed for very low PGAs results unexpectedly non-negligible, probably due to the same reasons previously mentioned. It can be observed that a damage index of 0.2 is attained for PGA values around 0.15 g, while for PGA equal to 0.3 g the damage index is around 0.30–0.35 for both the whole sample of single-nave churches and the stone masonry ones only.

**Table 2** Values of correlation parameters  $\alpha$  and  $\beta$  of Eq. (2)

Dataset	$\alpha$	$\beta$	RSS (weighted)
single-nave churches (633)	0.25	2.10	0.0018
Stone masonry churches (403)	0.23	1.91	0.0025
Brick masonry churches (146)	0.14	1.68	0.0003



Dataset	$\alpha'$	$\beta'$	RSS (weighted)
Single-nave churches (633)	1.00	2.75	0.001
Stone masonry churches (403)	0.96	2.62	0.001

(b)

**Fig. 9** Observed and predicted mean damage vs. PGA for: **a** all single-nave churches; **b** stone masonry churches

The relation is not plotted for brick masonry churches, as the small number of available data (146 churches only), in relation to the limited PGA range covered by the observations (0.0–0.2 g), does not allow to properly evaluate the mean damage by means of a logarithmic curve.

As done for  $I_{MCS}$ , the mean damage values are grouped for representative PGA ranges and, for each range, the mean damage index of the  $n_c$  churches in that range is computed as follows:

$$i_{d,mean}(PGA) = \frac{\sum_{i=1}^{n_c} i_d(PGA)}{n_c} \tag{4}$$

The PGA ranges are fixed considering that the observed data are not uniformly distributed over the entire PGA interval. In particular, due to the limited extension of the geographical areas stricken by higher accelerations, high PGA ranges are characterized by smaller number of data. Therefore, the selected PGA ranges are smaller for lower accelerations, and larger for higher PGAs, i.e.: 0–0.1 g, 0.1–0.2 g, 0.2–0.4 g, 0.4–0.6 g, and 0.6–0.8 g.

The observational data are compared in Fig. 9 with the curves for the predicted mean damage index, obtained by means of a best fitting procedure. The interpolating hyperbolic laws have the same format of Eq. (2), but expressed as a function of PGA, instead of  $I_{MCS}$ :

$$i_D = 0.5(1 + \tanh(\alpha' \log(PGA) - \beta')) \tag{5}$$

The fitted values of  $\alpha'$  and  $\beta'$  and of the RSS parameter related to Eq. (5) are listed in Table 3. It is worth noting that, for both datasets, the curves demonstrate a very good matching with the observational data, since the RSS value is only 0.001 in both cases. Note that the theoretical laws are supposed to be valid for PGAs ranging between 0 and 0.8 g, since the maximum registered PGA is 0.75 g.

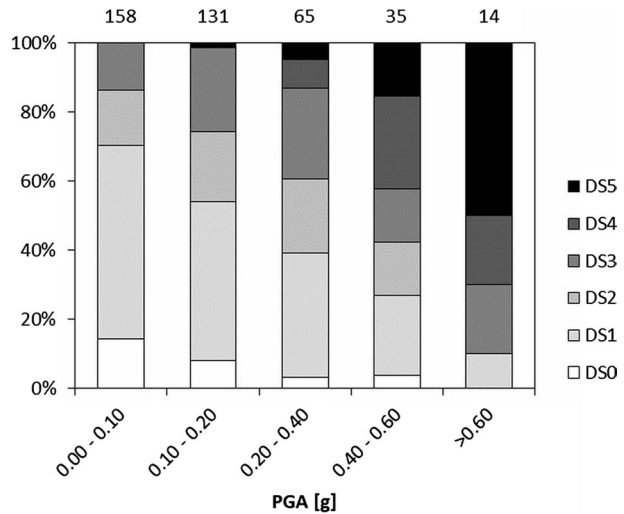
**Table 3** Values of correlation parameters  $\alpha'$  and  $\beta'$  of Eq. (5)

Dataset	$\alpha'$	$\beta'$	RSS (weighted)
Single-nave churches (633)	1.00	2.75	0.001
Stone masonry churches (403)	0.96	2.62	0.001

**Table 4** Correlation between the level of damage  $d_k$  and the ranges of the damage index  $i_d$

Damage index $i_d$ (Eq. (1))	Level of damage $DS_k$ (Lagomarsino and Podestà 2004b)
0.00–0.05	DS0
0.05–0.25	DS1
0.25–0.40	DS2
0.40–0.60	DS3
0.60–0.80	DS4
0.80–1.00	DS5

**Fig. 10** DPMs according to PGA ranges for single-nave stone masonry churches (403 cases)



### 4.3 Damage probability matrices (DPMs) for single-nave stone masonry churches

To obtain damage probability matrices (DPMs), it is necessary to transform the damage index given by Eq. (1) into a discrete variable according to the six damage levels of the EMS scale, and to correlate it to the specific PGA ranges defined in Sect. 4.2. The correlation between damage index and level of damage is summarized in Table 4.

Subsequently, DPMs are evaluated for the single-nave churches made of stone masonry only (403 cases). Figure 10 shows the damage distribution for each PGA interval for the selected churches, from which it emerges that most of these churches (72%) are characterized by  $PGA \leq 0.2$  g and about 40% by  $PGA \leq 0.1$  g. As expected, the damage distribution shows an increasing trend for higher seismic actions; in particular, for lower PGAs ( $\leq 0.1$  g), low to moderate damage levels (DS0 to DS3) are recorded, while for  $PGA > 0.3$  g, the percentage of low damage (DS0 and DS1) and higher damage levels (DS3, DS4, DS5) become more significant. These outcomes are used as background information for defining fragility curves for the subset of stone masonry churches, only.

## 5 Assessment of the mean damage for the most recurring mechanisms

### 5.1 Identification of the most recurring mechanisms

Thanks to the information about the damage levels related to each of the 28 mechanisms indicated in the A-DC form (PCM-DPC-MiBAC 2006), it is possible to analyse the correlation among the possible mechanisms, i.e. those that could be activated considering the typological and construction features in the analysed church, and their real activation (Fig. 11). Note that the mechanism is considered ‘activated’, if the damage level declared for it in the form is higher than or equal to D1.

Such an analysis can be useful to observe which are the most relevant mechanisms for the analysed class of single-nave masonry churches. In Fig. 11, the possible mechanisms are represented with blue or black bars, as percentages of the entire set of churches, while the percentage of activation for each mechanism, i.e. the mechanism occurrence as a percentage of each sample size of possible mechanisms, is represented with light blue or grey bars. This figure, thus, gives some valuable insight into the vulnerability of the churches in relation to each mechanism. Indeed, it shows the activation ratio for each mechanism, which is defined as the percentage of churches where the mechanism is activated over the entire set of churches in which that mechanism is possible. However, considering the relevance of the population dimension for the assessment of reliable vulnerability and fragility functions, only the most recurring mechanisms have been analysed here (i.e. the fourteen mechanisms represented by the blue and light blue bars in Fig. 11). Thus, the description of the most significant mechanisms for the investigated single-nave churches class is plotted in Fig. 12.

The following criterion is adopted for the choice of the most relevant mechanisms: those that simultaneously could be possible in at least 30% of the churches and are activated in more than 30% of the cases. Mechanism M25 (Interactions close to building irregularities) is not considered due to the very generic description of the mechanism, that makes the information in the survey form not very reliable.

Within the mechanisms identified as relevant for the examined single-nave churches, the most frequent ones (more than 90%) are those related to the macro-element of the façade (i.e. M1—overturning of the façade, M2—overturning of the upper part of the façade, M3 – in plane mechanism of the façade) and those related to the nave (i.e. M5 and

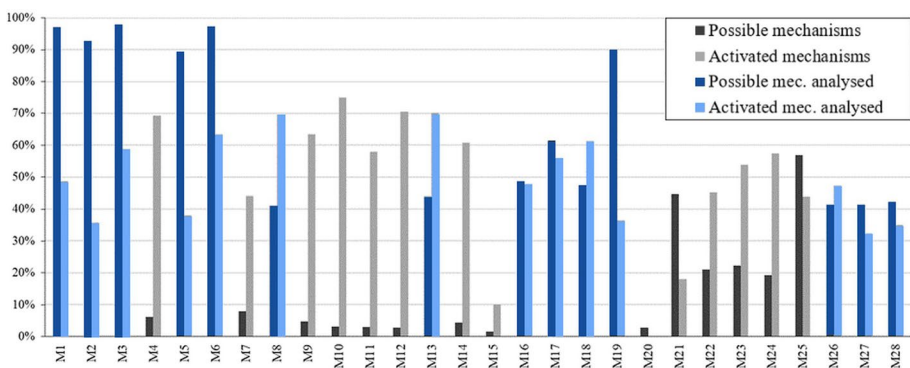
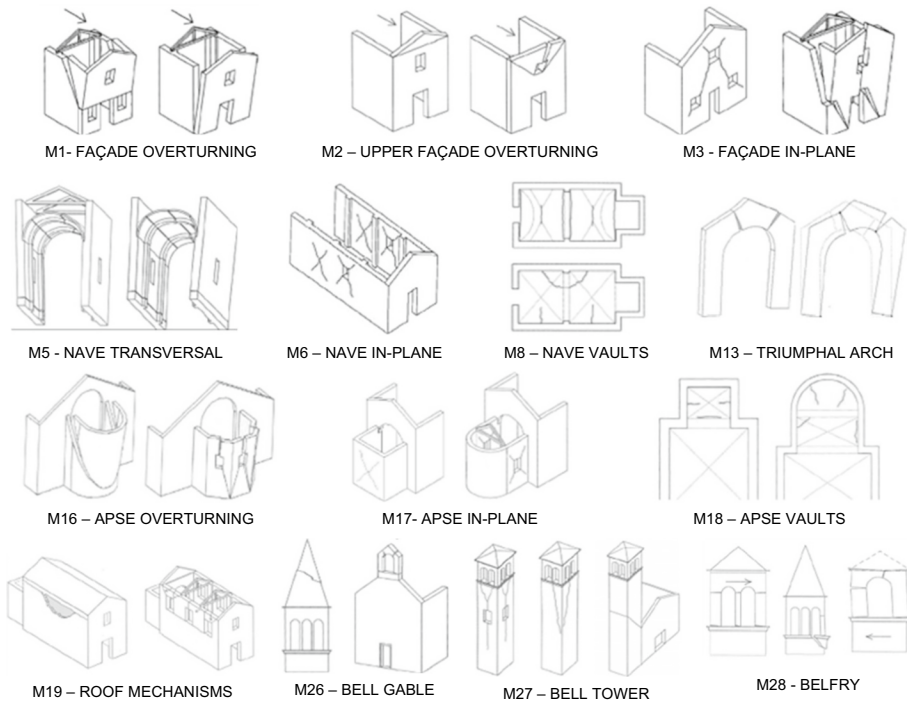


Fig. 11 Possible and activated mechanisms for the single-nave churches class



**Fig. 12** Analysed mechanisms (adapted from PCM-DPC-MiBAC 2006)

M6, transversal and in-plane mechanisms of the nave, respectively). Another very frequent mechanism is M19 (possible in 90% of cases and activated in around 38%), which is still related to the nave, but refers to the roof mechanisms. Further mechanisms related to the church nave, very often present (40–42%) and easily activated (70%), refer to the vaulted systems of the nave (M8) and to the triumphal arch (M13).

Additionally, in these very simple churches, the mechanisms related to bell gables (M26) or bell towers (M27 and M28) are also frequent (40%) and quite easily activated (30–48%).

Lastly, although the mechanisms related to the apse (M16, M17, M18) are less frequent (48–60%), as they concern only the second plan shape of Fig. 1, such a macro-element is interesting to be studied, considering the significant activation rate (around 50–60%) of the related mechanisms.

Starting from these considerations, accurate investigations on each of the most recurring mechanisms are carried out in the following. The damage level and the damage index for each mechanism are evaluated and compared with the overall damage previously discussed. Moreover, groups of mechanisms related to the same macro-element are compared in terms of vulnerability curves, i.e. considering the damage index versus either macro-seismic intensity or peak ground acceleration values.

## 5.2 DPMs for the most recurring mechanisms

First, as already developed for the global damage, the DPMs related to the highest PGAs recorded on each masonry church before the survey, without distinction between stone and

clay bricks, are computed with reference to the above-selected mechanisms and are plotted in Fig. 13. As in the case of Fig. 10, the damage distribution has an increasing trend for increasing seismic actions. These outcomes are used as background information for defining fragility curves for some of the selected mechanisms.

### 5.3 Assessment of mean damage index for the façade: mechanisms M1, M2 and M3

The observed and predicted mean damage referred to the mechanisms of the façade, i.e. M1, M2 and M3, are plotted in terms of macro-seismic (Fig. 14a) and PGA (Fig. 14b) intensities. As a comparison, the observed and predicted values of the global damage referred to the examined churches are reported in the same figures. The predicted mean damage for each mechanism is calculated again by means of Eq. (2) and Eq. (5) in function of  $I_{MCS}$  and PGA, respectively. Thus, the coefficients  $\alpha$  and  $\beta$  refer to the best fitting procedure of Eq. (2) in the  $I_{MCS}$  domain, whereas the coefficients  $\alpha'$  and  $\beta'$  refer to the best fitting of Eq. (5) in the PGA domain. Table 5 summarizes the values of all the correlation parameters, included the RSS values.

From the comparison of the three analysed mechanisms, it emerges that the in-plane mechanism of the façade (M3) is slightly more vulnerable than the out-of-plane ones (M1 and M2), both in terms of  $I_{MCS}$  and PGA. This outcome, that in general could seem quite surprisingly, should be interpreted in relation with the relevant frequency of occurrence of earthquakes in the geographical area under study. Past seismic events might have led, indeed, to a diffuse presence of ties and/or other earthquake-resistant details and interventions that improved building connections and avoided or mitigated the activation of out-of-plane mechanisms. Conversely, the comparison of the façade vulnerability with that of the entire church does not provide robust information, since in the  $I_{MCS}$  domain it is smaller than that of the entire church, whereas in the PGA domain the opposite trend can be observed. However, these differences are quite limited and can be also ascribable to the not exact correspondence between the macro-seismic intensity and peak ground acceleration that, for each church, are obtained independently. In fact, as mentioned above, the PGAs are evaluated by shake-maps interpolation, whereas the  $I_{MCS}$  are derived from the INGV reports.

Also, it can be noted that the damage indexes calculated in the  $I_{MCS}$  and PGA domains for the mechanisms involving the façade are quite similar to those related to the global damage to the church, especially in the PGA domain, and, thus, the vulnerability of the façade can be assumed emblematic of church average vulnerability.

### 5.4 Assessment of mean damage index for the nave: mechanisms M5, M6, M8 and M13

For the nave, four mechanisms contributing to its damage can be identified: M5, transversal mechanism, M6, in-plane mechanism, M8, damage to vaults, and M13, damage to the triumphal arch. According to the same fitting procedure involving Eq. (2) and Eq. (5), the couples of parameters  $\alpha$ ,  $\beta$  and  $\alpha'$ ,  $\beta'$  for the nave mechanisms and the corresponding RSS values are listed in Table 6. Figure 15 reports the observed and predicted values of the mean damage in terms of  $I_{MCS}$  (Fig. 15a) and PGA (Fig. 15b).

Figure 15 shows that the average response of the nave is similar to that of the whole church both in terms of  $I_{MCS}$  and PGA, even if the vulnerabilities of the single mechanisms

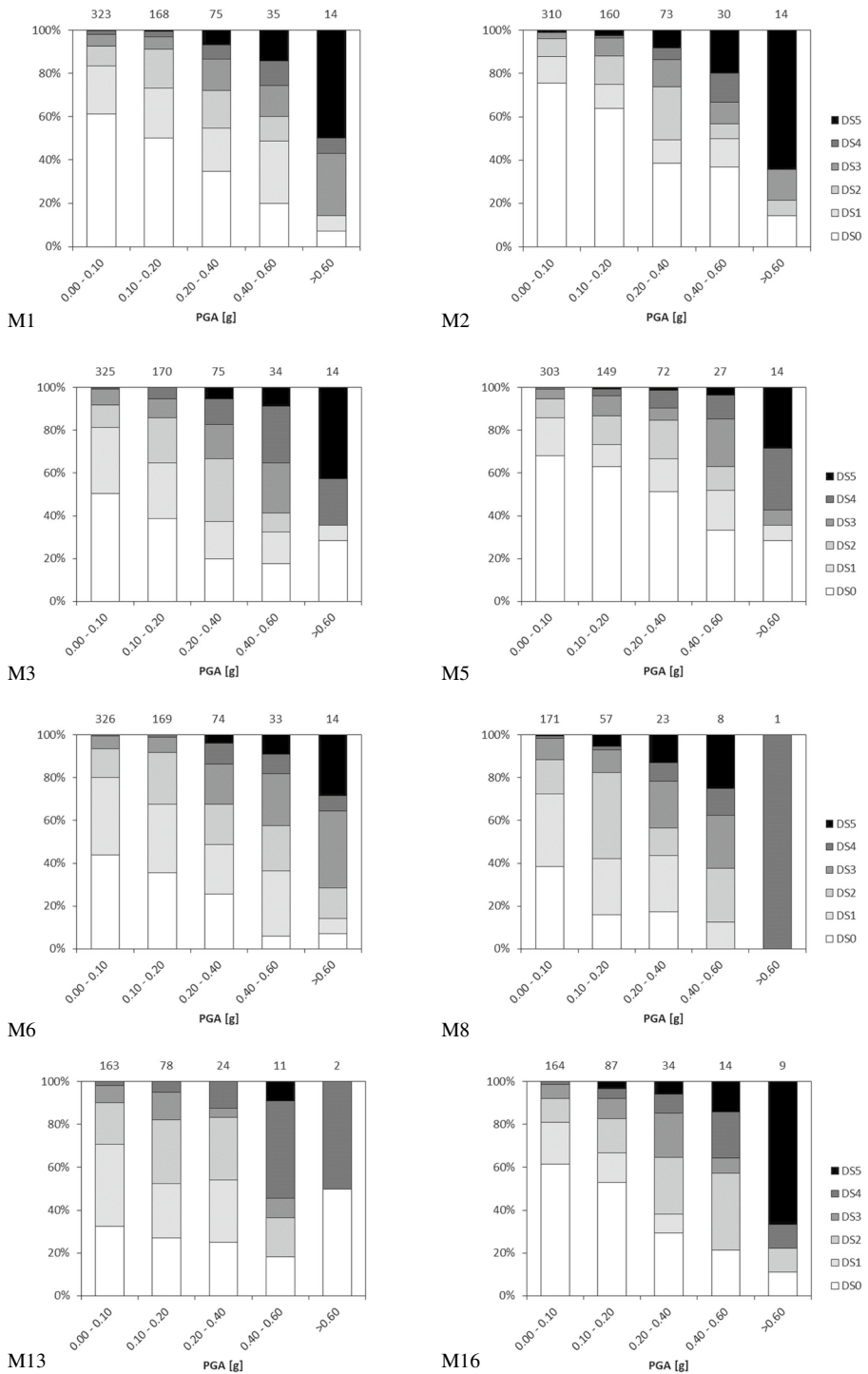


Fig. 13 DPMs for selected mechanisms in single-nave masonry churches



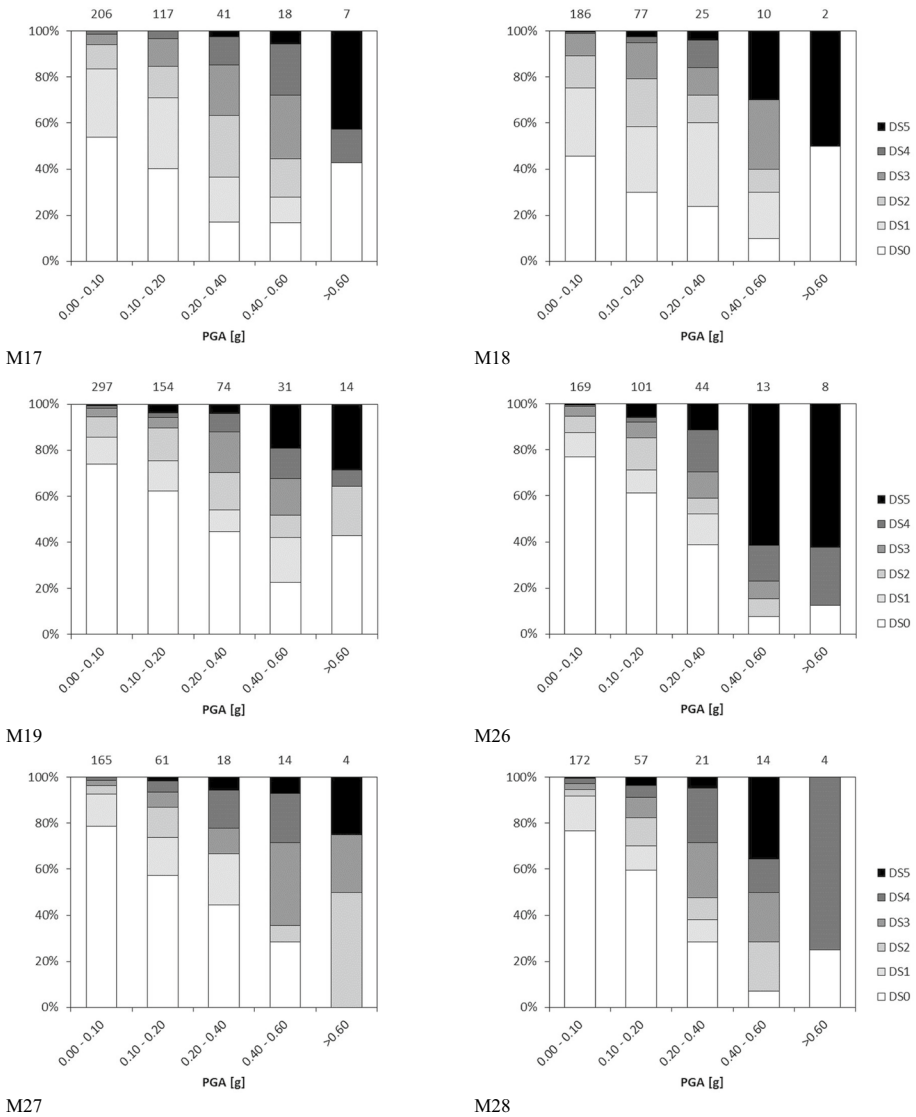
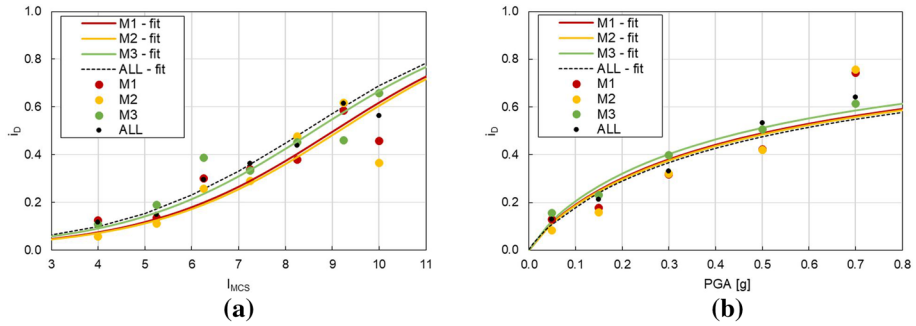


Fig. 13 (continued)

are quite differentiated compared to their average behaviour. The coincidence of the average behaviour of the nave with that of the whole church is probably due to the relevance of the related mechanisms in very simple churches, as the ones considered in the investigated dataset, which are, indeed, characterized by the presence of few other macro-elements. Both Fig. 15a and Fig. 15b show that the damage related to the transversal mechanism of the entire church (M5) is in general smaller, whereas the mechanism related to damage to nave vaults (M8) is definitely higher than church mean damage. Conversely, the in-plane mechanism along the nave lateral walls (M6) and the damage to the triumphal arch (M13) are closer to church mean damage both in terms of  $I_{MCS}$  and PGA. However, in terms of



**Fig. 14** Observed and predicted mean damage index for mechanisms M1, M2 and M3 and for the whole church in terms of: **a**  $I_{MCS}$ ; **b** PGA

**Table 5** Values of correlation parameters for the mean damage index of M1, M2 and M3

Mechanism	$i_D$ vs. $I_{MCS}$			$i_D$ vs. PGA		
	$\alpha$	$\beta$	RSS	$\alpha'$	$\beta'$	RSS
M1	0.25	2.26	0.05	1.00	2.72	0.05
M2	0.25	2.29	0.08	1.00	2.73	0.06
M3	0.25	2.15	0.04	1.00	2.68	0.00

**Table 6** Values of correlation parameters for the mean damage index of M5, M6, M8 and M13

Mechanism	$i_D$ vs. $I_{MCS}$			$i_D$ vs. PGA		
	$\alpha$	$\beta'$	RSS	$\alpha'$	$\beta'$	RSS
M5	0.25	2.38	0.01	1.00	2.93	0.02
M6	0.25	2.24	0.07	1.00	2.73	0.01
M8	0.22	1.65	0.01	0.83	2.01	0.03
M13	0.21	1.77	0.05	0.79	2.22	0.04

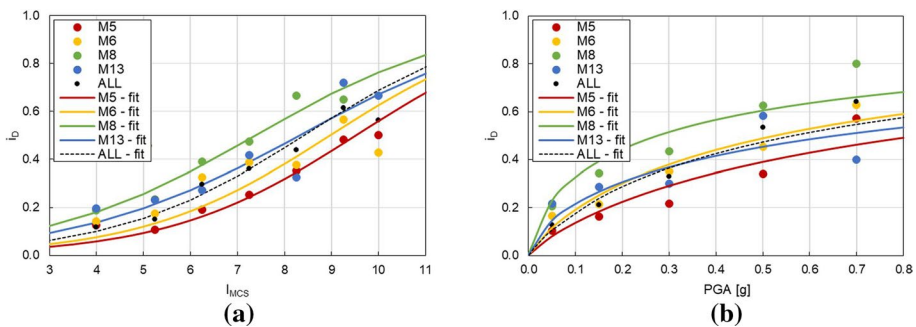


**Fig. 15** Observed and predicted mean damage index for mechanism M5, M6, M8 and M13 and for the whole church in terms of: **a**  $I_{MCS}$ ; **b** PGA

**Table 7** Values of correlation parameters for the mean damage index of M16, M17 and M18

Mechanism	$i_D$ vs. $I_{MCS}$			$i_D$ vs. PGA		
	$\alpha$	$\beta$	RSS	$\alpha'$	$\beta'$	RSS
M16	0.23	1.96	0.10	1.00	2.61	0.04
M17	0.23	2.18	0.05	1.00	2.73	0.00
M18	0.23	1.87	0.12	1.00	2.72	0.02

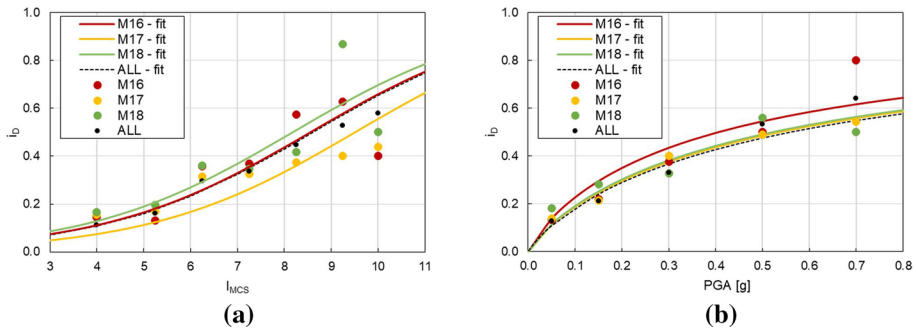


**Fig. 16** Observed and predicted mean damage index for mechanisms M16, M17 and M18, and for the whole church in terms of: **a**  $I_{MCS}$ , **b** PGA

$I_{MCS}$ , M6 is less vulnerable than M13 in the whole intensity range, while in terms of PGA, the differences are slighter and M6 provides lower vulnerability values than M13 only for PGA lower than 0.3 g.

### 5.5 Assessment of mean damage index for the apse: mechanisms M16, M17 and M18

Three mechanisms are related to the damage to ‘apse’ macro-element: the apse wall overturning (M16), the in-plane damage to apse wall (M17), and the damage to the vaults of the apse (M18). Table 7 lists the obtained values of the correlation parameters, whereas Fig. 16 reports the observed and predicted values of the mean damage in terms of  $I_{MCS}$  (Fig. 16a) and PGA (Fig. 16b). The fitting procedure is the same as the one described in Sect. 5.3 and 5.4.

The data and the curves plotted in both Fig. 16a and b do not show an evident trend. In terms of  $I_{MCS}$ , Fig. 16a seems to show that, similarly to what happens in the nave, the mechanism related to the vaults (M18) is the most vulnerable among the three ones. On the contrary, Fig. 16b shows that, in terms of PGA, M18 has a lower vulnerability compared to that of the whole church. Only for mechanism M17, the curves in the two domains are in good agreement, since they both provide a smaller vulnerability than M16 and M18. However, it should be noted that, in the case of apses, it is often difficult to distinguish between in-plane and out-of-plane mechanisms, since cracks have similar shapes and appears in similar positions unless in very specific cases. Therefore, it is not possible to give a final judgement about the performance of mechanisms M16 and M17.

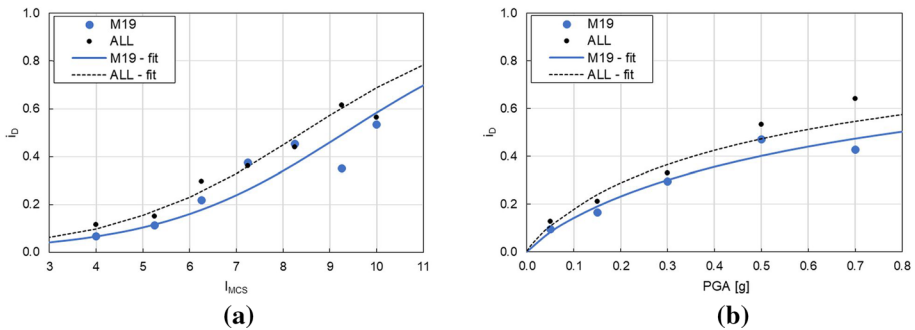
### 5.6 Assessment of mean damage index for the roof: mechanism M19

Table 7 lists the obtained values of the correlation parameters for the mechanism M19, related to the roof interaction with the nave, only. Figure 17 reports the observed and predicted values of the mean damage in terms of  $I_{MCS}$  (Fig. 17a) and PGA (Fig. 17b). For M19, both in the  $I_{MCS}$  and in the PGA domain, the fitting procedures on the observational data highlight a lower vulnerability of this mechanism compared to the average behaviour of the whole church (Table 8).

### 5.7 Assessment of mean damage index for the bell tower: mechanisms M26, M27 and M28

Three damage mechanisms are related to the bell tower or the bell gable: damage to the bell gable (M26), damage to the bell tower (M27), damage to the belfry (M28). Table 9 lists the obtained values of the correlation parameters for the mean damage indexes for each mechanism, obtained as already explained. Figure 18 reports the observed and predicted values of the mean damage in terms of  $I_{MCS}$  (Fig. 18a) and PGA (Fig. 18b).

The predicted curves of Fig. 18 are rather interesting as they confirm some “common sense” evaluations based on in-situ inspections, but supported by a quantitative analysis.



**Fig. 17** Observed and predicted mean damage index for mechanism M19, and for the whole church in terms of: **a**  $I_{MCS}$ , **b** PGA

**Table 8** Values of correlation parameters for the mean damage index of M19

Mechanism	$i_D$ vs. $I_{MCS}$			$i_D$ vs. PGA		
	$\alpha$	$\beta$	RSS	$\alpha'$	$\beta'$	RSS
M19	0.25	2.33	0.04	1.00	2.90	0.01

**Table 9** Values of correlation parameters for the mean damage index of M26, M27 and M28

Mechanism	$i_D$ versus $I_{MCS}$			$i_D$ vs. PGA		
	$\alpha$	$\beta$	RSS	$\alpha'$	$\beta'$	RSS
M26	0.25	1.97	0.14	0.99	2.50	0.06
M27	0.25	2.08	0.04	0.89	2.54	0.01
M28	0.25	1.87	0.06	0.89	2.22	0.08

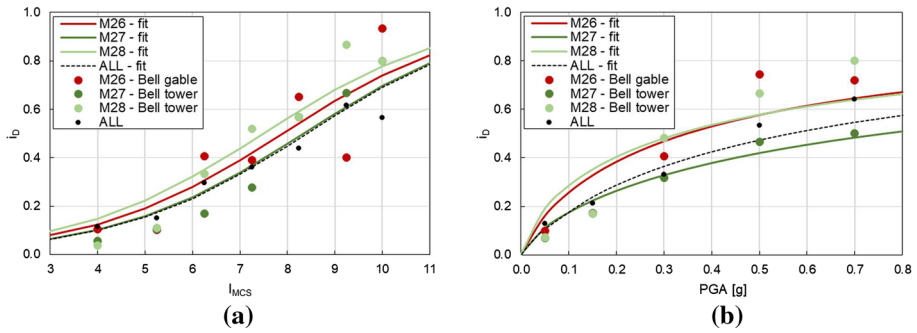


**Fig. 18** Observed and predicted mean damage index for the mechanism M26, M27 and M28, and for the whole church in terms of: **a**  $I_{MCS}$ , **b** PGA

First, both in terms of  $I_{MCS}$  and PGA, it is possible to observe that the bell gable (M26) and the belfry (M28) are very vulnerable in comparison with the whole church. On the other hand, the vulnerability of the bell tower (M27) is smaller than that of its belfry (M28) and it is also similar in terms of  $I_{MCS}$ , or even smaller in terms of PGA, than that of the entire church.

**5.8 Summary of mechanisms vulnerability**

Firstly, the analyses presented in the previous sections have highlighted that in most cases lower values of the parameter RSS are attained for the vulnerability curves in terms of PGA in comparison with the ones in terms of  $I_{MCS}$ . This evidences a higher reliability of the PGA measures. Then, the role of the coefficients  $\alpha$  and  $\beta$  in Eq. (2) is also herein pointed out.

The parameter  $\alpha$ , which is often called in the literature as  $1/q$  (Sandi and Floricel 1994, Lagomarsino and Podestà 2004b), is generally used as a constant value for a typological dataset and defines the slope of the curve. Conversely, the parameter  $\beta$  may be used to define the vulnerability level for the specific analysed dataset, since, for a given value of  $\alpha$ , it gives the height of the curve. This means that lower values of  $\beta$  deliver more vulnerable curves, whereas higher values of  $\beta$  deliver less vulnerable curves. In this context, defined  $\bar{\beta}$  as the value obtained by the best fitting on the damage index related to the entire church, and  $\beta_i$  the value obtained for the single mechanism, a distance factor  $\epsilon_{\beta,i}$  for the  $i$ -th analysed mechanism is defined as follows:

$$\epsilon_{\beta,i} = \frac{\beta_i - \bar{\beta}}{\bar{\beta}} \tag{7}$$

If this parameter is positive, the  $i$ -th mechanism is less vulnerable than the overall church, whereas when it is negative, the  $i$ -th mechanism is more vulnerable than the overall church. Figure 19 provides an overview of the distance factor for the 14 analysed mechanisms calculated with reference to both  $I_{MCS}$  and PGA, in order to summarize the above-mentioned results.

As already mentioned, it is possible to observe that, besides mechanisms M16 and M18, for which the results in terms of  $I_{MCS}$  or PGA give some inconsistencies, for all the other

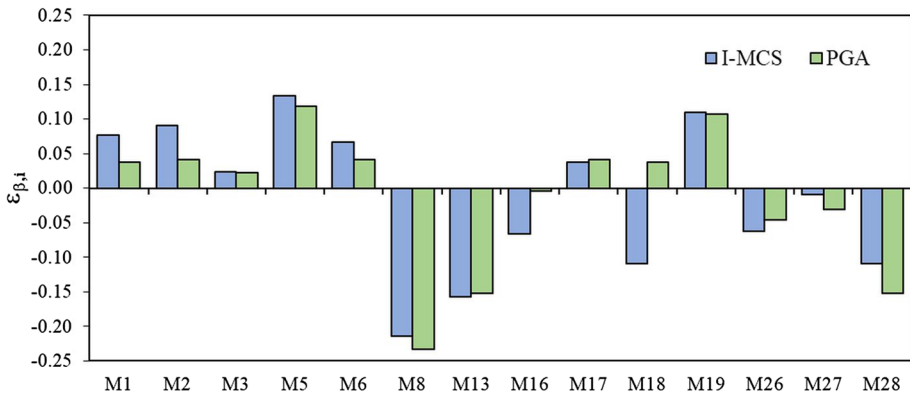


**Fig. 19** Mean damage index of the analysed mechanisms (with baseline fixed at the mean damage index of churches)

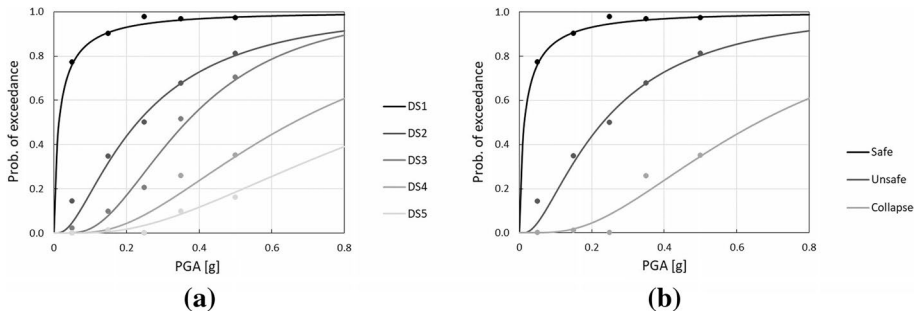
mechanisms there is a good agreement between the two evaluations. Therefore, it is possible to conclude that the six main mechanisms related to the simple church configuration, such as the overturning (M1 and M2) and the in-plane (M3) mechanisms of the façade, the transversal (M5) and the in-plane (M6) mechanisms of the nave, and the mechanism related to the interaction of the roof with the nave (M19) are less vulnerable than the other ones, being their vulnerability quite similar (in the case of M1, M2, M3, and M6) or even significantly smaller (M5, M19) than the global vulnerability of the whole church.

Figure 19 also shows that the most vulnerable mechanisms are those related to damage to the vaults of the nave (M8) and to the triumphal arches (M13), characterized, indeed, by a vulnerability that is higher than that of the whole church. Moreover, this representation confirms that the mechanisms related to the presence of bell towers and/or bell gable (M26, M27, M28) are more vulnerable than the whole church, with a very significant contribution to vulnerability given by the mechanism related to the belfry (M28).

## 6 Fragility curves

### 6.1 Fragility curves related to global damage for single-nave churches class

Fragility curves are developed in this section with reference to the global damage observed for the single-nave churches class (633 churches). The starting data are represented again by the global damage indexes collected by means of the A-DC forms and the correlations reported in Table 4 are considered for defining the damage state achieved by each church of the class. Cumulative distribution functions in terms of PGA are, thus, evaluated for each damage state. The curves fitting the observational data have a lognormal distribution and are obtained through a statistical method available in the literature, i.e. the maximum likelihood approach (Baker 2015). To perform the fitting, significant PGA intervals are defined as: 0.0–0.1 g, 0.1–0.2 g, 0.2–0.4 g, 0.4–0.6 g, and 0.6–0.8 g. On the contrary, for the analysis of the whole dataset related to the entire church and in order to carry out a comparison with the previous study (Cescatti et al. 2020), a further subdivision of the interval 0.2–0.4 g (i.e. 0.2–0.3 g, 0.3–0.4 g) is assumed.



**Fig. 20** Fragility curves for single-nave masonry churches: **a** all damage states; **b** merged damage states

**Table 10** Parameters of the obtained empirical fragility curves (Cescatti et al. 2020)

	DS1	DS2	DS3	DS4	DS5
$\theta$	0.014	0.230	0.364	0.660	0.988
$\delta$	1.79	0.91	0.63	0.70	0.76
$\eta$ – Likelihood	–9.1	–10.0	–10.0	–6.0	–4.8

Being the fragility defined as the probability of exceeding a given damage state, the curves reported in Fig. 20 represent the probability of having a damage higher than or equal to a certain damage level. Figure 20a shows the fragility curves and the observational data used for their fitting with reference to all the damage states, while Fig. 20b summarizes the experimental and the predicted damage in three main conditions that, from a civil protection point of view and for a very fast estimate of the losses associated with a certain event, could bring to simplified and immediate results. In particular, the following reference damage states are defined:

- Slight damage/safe: DS1
- Moderate damage/unsafe: DS2
- Severe damage/collapse: DS4

As presented in the analysis of the usability outcomes related to the damage levels for the presented dataset (Cescatti et al. 2020), most churches with damage level higher than or equal to DS2 were defined as ‘unsafe’ and the churches with damage level higher than or equal to DS4 were defined as ‘severely damaged’ or ‘near to collapse’.

Table 10 summarizes the mean value,  $\theta$ , and the standard deviation,  $\delta$ , of the logarithmic functions plotted in Fig. 20 and the interpolations of the observational points for each damage state. The errors,  $\eta$ , between the theoretical values and the observational ones are also listed in this table and represent the likelihood parameter. These data, already presented in (Cescatti et al. 2020), are herein reported only for the sake of comparison with the damage and collapse mechanisms presented in the following subsection.

## 6.2 Fragility curves related to the most recurring mechanisms

In this section, fragility curves related to single mechanisms are presented with the aim of comparing the vulnerability of the most recurring mechanisms with the global vulnerability of the church at different damage states, and not only in terms of mean damage (as in Sect. 5). The procedure for obtaining the fragility curves for the mechanisms is the same adopted in Sect. 6.1.

Since the definition of six damage states (from DS0 to DS5) requires a high number of observations to obtain reliable results, only the most frequent mechanisms are analysed. In particular, among the mechanisms having a percentage of activation higher than 90% (see Fig. 11), the following ones are selected: the out-of-plane mechanisms of the façade M1 (615 cases), the transversal response of the nave M5 (618 cases), the two main in-plane mechanisms of the façade M3 (565 cases) and of the nave M6 (616 cases). These mechanisms are, indeed, related to the macro-elements (façade and lateral walls) that constitute the basic “structure” of the church and thus, frequently occur. Moreover, in Sect. 5.8, it has been evidenced that these mechanisms generally have a vulnerability similar to or slightly lower than that of the church. The data refer to the single-nave churches for which the selected mechanisms are possible.

Table 11 lists the significant parameters (mean value, standard deviation, error) of the logarithmic laws obtained for the selected mechanisms. Figure 21 reports, for each mechanism, the fragility curves for all the damage states (Figure 21a) and those corresponding to the three reference damage conditions for defining usability (i.e. DS1, DS2, and DS4, Figure 21b). The observational points used for the data fitting are also reported, as already done for the global behaviour in the previous subsection.

The fragility curves for mechanism M1 (overturning of the façade) are plotted in Fig. 21a and b. Comparing Fig. 21a with Fig. 20a, it is clear that for slight to moderate damage states (DS1 to DS3), M1 has a lower probability of exceeding these states than the whole structure, for any value of PGA. On the other hand, for the severe damage/collapse state, and particularly for the most severe one (DS5), the probability of exceedance for M1 and for the whole church is almost the same. Figure 21a shows that for lower values of PGAs the observational points are well interpolated by the logarithmic curves, whereas for higher values of PGAs (i.e.  $PGA \geq 0.4$  g) the points deviate significantly from the curves. Figure 21c and d show the fragility curves obtained for the in-plane mechanism of the façade (M3). The comparison between Fig. 21c and Fig. 20a shows that for any damage state (DS1 to DS5), M3 has a lower probability of exceeding the damage states than the whole structure, for any value of PGA.

**Table 11** Parameters of the obtained empirical fragility curves for M1, M3, M5, and M6

	M1			M3			M5			M6		
	$\theta$	$\delta$	$\eta$	$\theta$	$\delta$	$\eta$	$\theta$	$\delta$	$\eta$	$\theta$	$\eta\delta$	$\eta$
DS1	0.109	2.386	-13.57	0.054	2.719	-13.20	0.295	3.478	-13.51	0.036	2.844	-13.89
DS2	0.404	2.032	-14.30	0.240	1.725	-13.19	0.626	2.329	-11.80	0.284	1.951	-13.36
DS3	0.835	1.762	-20.14	0.591	1.655	-15.03	1.169	1.886	-13.55	0.761	1.632	-17.59
DS4	1.310	1.410	-13.53	0.749	1.064	-10.57	1.252	1.230	-10.89	1.324	1.179	-10.41
DS5	1.174	0.950	-10.20	1.474	0.993	-10.58	1.604	0.859	-6.10	1.070	0.661	-5.07



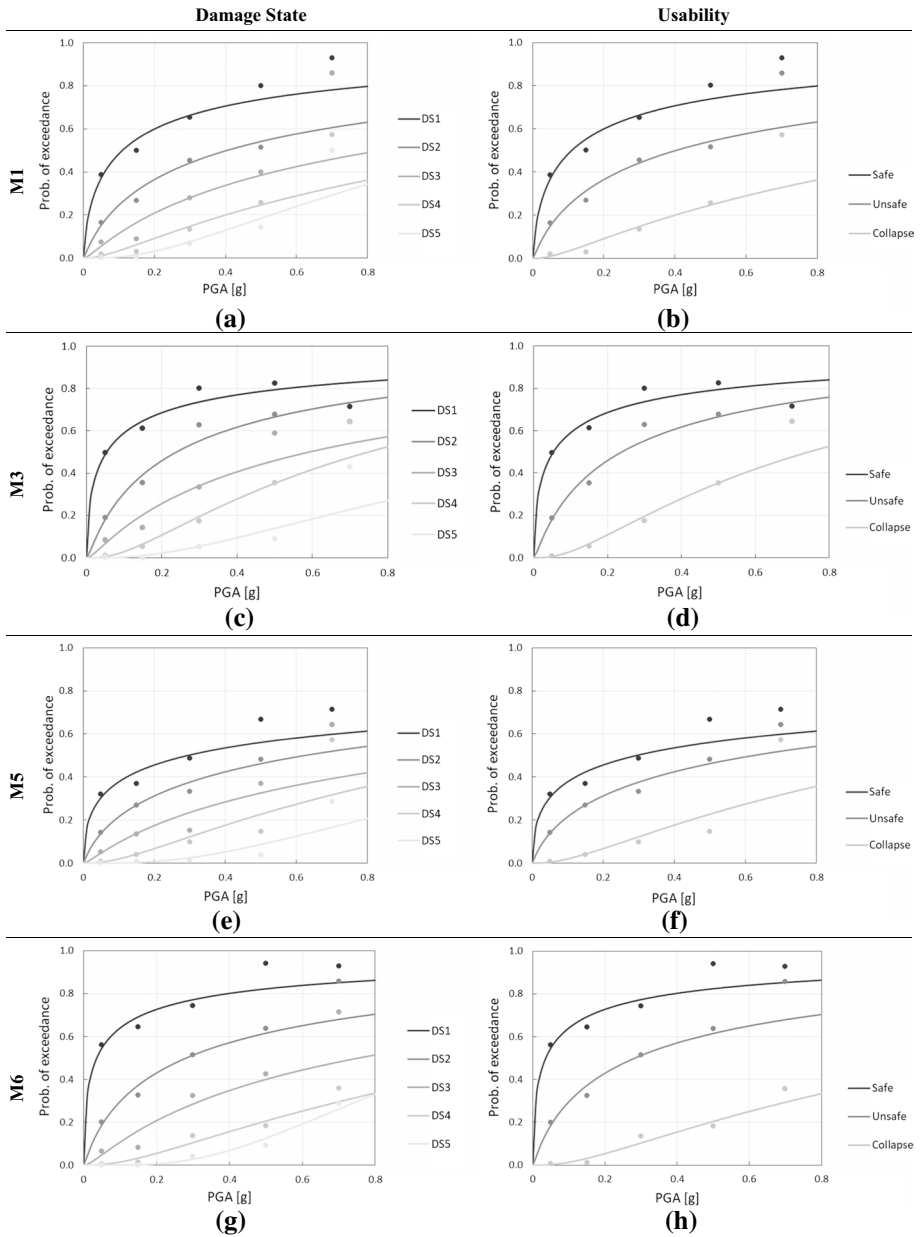


**Fig. 21** Fragility curves for the mechanisms M1, M3, M5 and M6: all damage levels and reference damage levels

The comparison between the fragility curves for M3 (Fig. 21c,d) and M1 (Fig. 21a,b) confirms the general observations based on the vulnerability curves and reported in Sect. 2.3. The probability of damage for M3 is, indeed, higher than that of M1, in particular for lower levels of damage (DS1 to DS3). As previously observed, such a limited

vulnerability of M1 might be due to the presence of earthquake-resistant details or past interventions able to improve the connections in the church and reduce the vulnerability to out-of-plane actions until DS3. Conversely, for higher damage states, i.e. near collapse and collapse, the trend is inverted, because, when the connections fail, the overturning mechanism develops with more severe damage.

Figure 21e and f show the fragility curves obtained for the transversal mechanism of the nave (M5) and highlight that the damage probability of M5 is significantly lower than that of the previously analysed mechanisms and of the entire church, whatever the damage state is. This mechanism is, thus, less vulnerable than others, as also the graphs of Figs. 15 and 19 evidence, both in terms of PGA and  $I_{MCS}$ . It is also significant that this mechanism entails the onset of overturning for the lateral walls of the nave but, since it activates the entire church in the transversal response, it is less vulnerable than the single façade overturning (M1). This trend is confirmed also for the highest damage states and is reasonable, because the attainment of DS5 for M5 means the complete collapse of the church.

Finally, Figure 21 g and Figure 21 h show that the probability of having in-plane shear damage to the lateral walls of the nave (M6) is higher than the probability of damage related to the transversal behaviour of the nave (M5), particularly for the lower damage states (DS1 to DS3). Such a trend is inverted for the severe damage/near collapse state DS4, where the probability of exceedance become lower for M6 than for M5. This result completely confirms the trend already observed for in-plane (M3) and out-of-plane (M1) mechanisms of the façade.

## 7 Conclusions

This paper developed detailed analyses on a database of churches gathered after the 2016–17 Central Italy seismic sequence. First, the typological description of the dataset allowed highlighting that the area is mainly characterised by the presence of small churches, with rectangular shape, having sometimes apse, and with a gabled façade. Since more complex church shapes and churches with high dimensions are seldom present and, therefore, statistically less significant, they were not considered in this study. Masonry typology varies between brick masonry, mainly along the sea coast, and irregular stone masonry, generally located at higher altitudes on the Apennines. The statistical analysis of the database also evidenced that the bell gable is more characteristic of smaller churches, with a volume lower than 800–1000 m<sup>3</sup>, whereas churches bigger than 1500 m<sup>3</sup> generally have a bell tower. Bell towers, in this type of churches, are generally integrated or partially integrated within the church building, whereas isolated bell towers are not typical in the investigated area. Examination of the main typological characteristic of the churches in the database allowed identifying a homogeneous class of churches; for such a class, the most recurring damage and collapse mechanisms were identified and evaluated, and a specific analysis of their vulnerability was carried out to overcome the simplistic description of the overall church behaviour related to the global mean damage index only, as usually analysed in the literature. In particular, the sources of actual vulnerability (i.e. the most vulnerable mechanisms) were analysed more in detail, with the aim of: i) identifying which vulnerable mechanisms need to be examined more in detail in the post-seismic surveys, and ii) understanding which local interventions might mitigate the seismic risk of this church type. This is an original contribution of the paper in the field of the vulnerability assessment of

masonry churches, since there is still little information in the literature concerning both the damage levels related to specific mechanisms and their influence on the overall damage of the whole church.

Moreover, a better knowledge related to each single damage mechanism could be a first step to eventually improve the overall church damage index calculation, which is currently based on as a simple average of the damage level attained by each mechanism.

The analysis of the dataset, in terms of damage and collapse mechanisms, allowed to identify six more relevant mechanisms: complete (M1) or partial (M2) overturning of the façade, in-plane mechanism of the façade (M3), transversal (M5) and in-plane (M6) mechanism of the entire church, roof interaction with the nave (M19). These mechanisms showed in general damage indexes that are smaller than those referred to the entire church. It is worth noting that the macro-elements to which these mechanisms are related constitute the basic “structure” of the church.

Conversely, some mechanisms typical of the presence of specific macro-elements, such as vaults and triumphal arches (M8, M13, M18), or bell gable and bell tower (M26, M27, M28), proved to be more vulnerable compared to overall church behaviour. Particularly, it was observed that bell gables and belfries are more vulnerable than bell towers, but overall, these three mechanisms are all more vulnerable when compared with the overall behaviour of the church. This is quite important from the point of view of safety, because a significant probability of collapse for bell gables, belfries and non-isolated bell towers could induce damage to the rest of the church, threatening the safety of the entire church and worsening the global damage level. Conversely, targeted interventions on these elements could limit their vulnerability and improve the global safety of the church.

The analysis of the fragility curves for the mechanisms related to the transversal and in-plane behaviours of both the façade (M1 and M3) and the nave (M5 and M6) evidenced in general a smaller fragility of these mechanisms compared with the whole church for all the damage states, with the exception of M1 for the highest damage states. In addition, it seems that, for a defined PGA level, the in-plane mechanisms (M3 and M6) have a higher probability of exceeding the lower damage states (DS1 to DS3) than the out-of-plane ones, probably because of existing connections among structural elements, which were able to avoid overturning and to promote the onset of shear cracks at the lowest damage states. Conversely, for severe damage state (DS4), the overturning mechanisms, which might yield to the complete collapse of the elements, have higher probability of exceedance.

The adopted approach presented in this paper is effective to give insights into church seismic behaviour, with a special focus on the damage related to single mechanisms, generally less investigated than the global damage. The same application on an enlarged dataset might improve the reliability of the fragility curves and the evaluation of vulnerability for the mechanisms herein studied. Moreover, a more extended dataset could allow a significant analysis of all the mechanisms from a statistical point of view, even those not investigated here, and of the global vulnerability of each macro-element, characterized by the possible activation of more than one mechanism.

**Acknowledgements** Authors want to acknowledge MiC (Italian Ministry of Culture), DPC (Department of Civil Protection) and ReLUIIS (Network of University Laboratories of Seismic and Structural Engineering) for giving the possibility to help in the emergency phase and to analyse the gathered dataset. This study has been supported by a program funded by the Presidency of the Council of Ministers, Italian Department of Civil Protection (2022–2024 DPC-ReLUIIS).

**Funding** Open access funding provided by Università degli Studi di Napoli Federico II within the CRUI-CARE Agreement. This article has been developed under the financial support of the Italian Department of Civil Protection, within the ReLUIS-DPC 2022–24 Research Project.

## Declarations

**Conflicts of interest** The authors declare that they have no conflict of interest.

**Open Access** This article is licensed under a Creative Commons Attribution 4.0 International License, which permits use, sharing, adaptation, distribution and reproduction in any medium or format, as long as you give appropriate credit to the original author(s) and the source, provide a link to the Creative Commons licence, and indicate if changes were made. The images or other third party material in this article are included in the article's Creative Commons licence, unless indicated otherwise in a credit line to the material. If material is not included in the article's Creative Commons licence and your intended use is not permitted by statutory regulation or exceeds the permitted use, you will need to obtain permission directly from the copyright holder. To view a copy of this licence, visit <http://creativecommons.org/licenses/by/4.0/>.

## References

- Baker J (2015) Efficient analytical fragility function fitting using dynamic structural analysis. *Earthq Spectra* 31(1):579–599
- Canuti C, Carbonari S, AstaDall A, Dezi L, Gara F, Leoni G, Morici M, Petrucci E, Prota A, Zona A (2021) Post-earthquake damage and vulnerability assessment of churches in the marche region struck by the 2016 central italy seismic sequence. *Int J Architec Herit* 15(7):1000–1021. <https://doi.org/10.1080/15583058.2019.1653403>
- Casapulla C, Argiento LU, Maione A, Speranza E (2021) Upgraded formulations for the onset of local mechanisms in multi-storey masonry buildings using limit analysis. *Structures* 31:380–394. <https://doi.org/10.1016/j.istruc.2020.11.083>
- Cescatti E (2016) Combined experimental and numerical approaches to the assessment of historical masonry structures Ph.D. Thesis, University of Trento
- Cescatti E, Follador V, da Porto F (2021) Typological analysis and vulnerability curves for masonry churches. In: *Proceedings of the 8th international conference on computational methods in structural dynamics and earthquake engineering methods in structural dynamics and earthquake engineering (COMPdyn 2021)*, Athene, Greece, June 28–30: 3141–3154 <https://doi.org/10.7712/120121.8702.19026>
- Cescatti E, Salzano P, Casapulla C, Ceroni F, da Porto F, Prota A (2020) Damages to masonry churches after 2016–2017 Central Italy seismic sequence and definition of fragility curves. *Bull Earthq Eng* 18(1):297–329. <https://doi.org/10.1007/s10518-019-00729-7>
- da Porto F, Silva F, Costa C (2009) Modena C (2012) Macro-scale analysis of damage to churches after earthquake in Abruzzo (Italy) on April 6. *J Earthquake Eng* 16(6):739–758
- D'Ayala D, Speranza E (2003) Definition of collapse mechanisms and seismic vulnerability of historic masonry buildings. *Earthq Spectra* 19(3):479–509
- De Matteis G, Brando G, Corlito V (2019) Predictive model for seismic vulnerability assessment of churches based on the 2009 L'Aquila earthquake. *Bull Earthq Eng* 17:4909–4936. <https://doi.org/10.1007/s10518-019-00656-7>
- De Matteis G, Zizi M (2019) Seismic damage prediction of masonry churches by a PGA-based approach. *Int J Architec Heritage* 13(7):1165–1179. <https://doi.org/10.1080/15583058.2019.1597215>
- Doglionni F, Moretti A, Petrini V, Angeletti P (1994) Le chiese e il terremoto. dalla vulnerabilità constatata nel terremoto dei friuli al miglioramento antisismico nel restauro, verso la politica di prevenzione. Trieste, Italy, Lint Editoriale Associati.
- DPCM (2011) Linee Guida per la valutazione e riduzione del rischio sismico del patrimonio culturale – allineamento alle nuove Norme tecniche per le costruzioni (relative al DM 14/ 01/2008). GU no. 47, 26/ 02/2011—Suppl. Ordinario no. 54.
- Giresini L, Casapulla C, Denysiuk R, Matos J, Sassu M (2018) Fragility curves for free and restrained rocking masonry façades in one-sided motion. *Eng Struct* 164:195–213. <https://doi.org/10.1016/j.engstruct.2018.03.003>

- GNDT-DISEG (2004) Decreto del 9 marzo 2004 n°26 nel Bollettino Ufficiale della Regione Molise, Supplemento ordinario n°1 al B.U.R.M., 1 settembre 2004, n°17. Approvazione "Linee guida preliminari per gli interventi di riparazione del danno e miglioramento sismico per gli edifici di culto e monumentali – EDIFICI DI CULTO – PARTE PRIMA"
- Lagomarsino S (2012) Damage assessment of churches after L'Aquila earthquake (2009). *Bull Earthq Eng* 10(1):73–92. <https://doi.org/10.1007/s10518-011-9307-x>
- Lagomarsino S, Podestà S (2004) Seismic vulnerability of ancient churches: I. damage assessment and emergency planning. *Earthq Spectra* 20(2):377–394
- Lagomarsino S, Podestà S (2004) Seismic vulnerability of ancient churches: II. statistical analysis of surveyed data and methods for risk analysis. *Earthq Spectra* 20(2):395–412
- Lagomarsino S, Cattari S, Ottonelli D, Giovinazzi S (2019) Earthquake damage assessment of masonry churches: proposal for rapid and detailed forms and derivation of empirical vulnerability curves. *Bull Earthq Eng* 17:3327–3364. <https://doi.org/10.1007/s10518-018-00542-8>
- Marotta A, Sorrentino L, Liberatore D, Ingham JM (2018) Seismic risk assessment of New Zealand unreinforced masonry churches using statistical procedures. *Int J Archit Heritage* 12(3):448–464. <https://doi.org/10.1080/15583058.2017.1323242>
- Marotta A, Liberatore D, Sorrentino L (2021) Development of parametric seismic fragility curves for historical churches. *Bull Earthq Eng* 19:5609–5641. <https://doi.org/10.1007/s10518-021-01174-1>
- MiBACT (Ministero dei Beni delle Attività Culturali e del Turismo) (2015) Direttiva 23 aprile 2015: Aggiornamento della direttiva 12 dicembre 2013, relativa alle "Procedure per la gestione delle attività di messa in sicurezza e salvaguardia del patrimonio culturale in caso di emergenze derivanti da calamità naturali. G.U. Serie Generale no. 169
- Morici M, Canuti C, Dall'Asta A, Leoni G, (2020) Empirical predictive model for seismic damage of historical churches. *Bull Earthq Eng* 18:6015–6037. <https://doi.org/10.1007/s10518-020-00903-2>
- Nale M, Minghini F, Chiozzi A, Tralli A (2021) Fragility functions for local failure mechanisms in unreinforced masonry buildings: a typological study in Ferrara, Italy. *Bull Earthq Eng* 19:6049–6079. <https://doi.org/10.1007/s10518-021-01199-6>
- PCM-DPC-MiBAC (Presidenza Consiglio dei Ministri-Dipartimento della Protezione Civile-Ministero dei Beni e Attività Culturali) (2006) Model A-DC Scheda per il rilievo del danno ai beni culturali—Chiese
- Penna A, Calderini C, Sorrentino L, Carocci C, Cescatti E, Sisti R, Borri A, Modena C, Prota A (2019) Damage to churches in the 2016 central Italy earthquakes. *Bull Earthq Eng* 17:5763–5790. <https://doi.org/10.1007/s10518-019-00594-4>
- Salzano P, Casapulla C, Ceroni F, Prota A (2022) Seismic vulnerability and simplified safety assessment of masonry churches in the Ischia Island (Italy) after the 2017 earthquake. *Int J Architect Heritage* 16(1):136–162. <https://doi.org/10.1080/15583058.2020.1759732>
- Sandi H, Floricel I (1994) Analysis of seismic risk affecting the existing building stock. Proceedings of the 10th European Conference on Earthquake Engineering, Vienna, 2: 1105–1110 A. A. Balkema, Rotterdam
- Sieberg A (1930) Scala MCS (Mercalli-Cancani-Sieberg). *Geologie Der Erdbeben, Handbuch Der Geophysik* 2:552–555
- Solarino F, Giresini L (2021) Fragility curves and seismic demand hazard analysis of rocking walls restrained by elasto-plastic ties. *Earthq Eng Struct Dynam* 50(13):3602–3622. <https://doi.org/10.1002/eqe.3524>
- Sorrentino L, Liberatore L, Decanini LD, Liberatore D (2014) The performance of churches in the 2012 emilia earthquakes. *Bull Earthq Eng* 12:2299–2331. <https://doi.org/10.1007/s10518-013-9519-3>
- Taffarel S, Giaretton M, da Porto F, Modena C (2016) Damage and vulnerability assessment of URM buildings after the 2012 Northern Italy earthquakes. In: Proceedings of the 16th International Brick and Block Masonry Conference (IBMAC 2016), Padua, Italy, June 26–30
- Zizi M, Rouhi J, Chisari C, Cacace D, De Matteis G (2021) Seismic vulnerability assessment for masonry churches: an overview on existing methodologies. *Buildings* 11(12):588. <https://doi.org/10.3390/buildings11120588>